FULL PAPER

An Effective Approach for the Development of Reliable YBCO Bulk Cryomagnets with High Trapped Field Performances

Driss Kenfaui, Pierre-Frédéric Sibeud, Eric Louradour, Xavier Chaud, and Jacques G. Noudem*

Widespread use of $YBa_2Cu_3O_{7-\delta}$ (Y123) bulk superconductors as source of strong magnetic fields requires development of high-performance materials sufficiently reliable with improved thermal transfer ability. An effective approach based primarily on the growth of bulk Y123 single domains comprising a holes-network to diminish the oxygen diffusion paths is reported here, as well as their progressive annealing at high temperature under oxygen pressure to reduce undue stresses and processing time. Finely, it aims to stimulate the thermal exchange inside the superconductor and compensate for induced magnetic stresses during the field-trapping process. The approach brings considerable time and energy savings, and turns out to knock down barriers having stymied hitherto the use of Y123 bulk superconductors for engineering applications. Indeed, it enables the achievement of a pore-free and crack-free microstructure yielding marked fracture toughness and promoting large size persistent current loops, thereby boosting the trapped field performances. The fostering of the internal thermal exchange leads the maximum trapped field B_{max} to shift to higher temperatures by up to 14 K. A value B_{max} of 6.34 T is attained at 17 K on ≈16 mm-diameter reinforced pellet (disk area $s = 1.99\ cm^2$), resulting in an outstanding field density $B_{max}/s = 3.19\ T\,cm^{-2}$.

1. Introduction

The three past decades have witnessed intensive research efforts devoted to the high temperature bulk superconductors (RE)-Ba-Cu-O (with RE is a rare-earth element) because of their ability to generate magnetic fields considerably stronger than those attainable with conventional permanent magnets.[1–4] Bulk (RE)-Ba-Cu-O single-grain (so-called single domain) superconductors cooled below their critical temperature under a magnetic activation trap and retain a part or almost all the applied field. They can be hence used as magnets as long as they are maintained at such low temperature levels, which makes them potentially useful for engineering applications such as strong permanent cryomagnets,[3–5] and compact and portable cryogenic motors and generators.[5,6] The trapped field, B, stems from the persistent currents macroscopically circulating in a (RE)-Ba-Cu-O superconductor and depicts a profile on the material surface culminating at a maximum B_{max} at the center with a field gradient toward the edge. Bean model stipulates that B_{max} is proportional to the critical current density J_c and the size of the persistent current loops.[7]

A great deal of research has been then broadly focused on the critical currents in the large $YBa_2Cu_3O_{7-\delta}$ (Y123) single domains that can be reproducibly fabricated by using a top-seeded melt growth (TSMG) process.[2–6] The critical current density J_c has been highly enhanced by incorporating defects into the crystal, which causes pinning by locally perturbing or destroying the superconducting properties. Doping the precursor material prior to crystal processing remains the primary approach used hitherto to introduce defects into bulk superconductors and resulted in very high trapped fields.[2,4] Gruss[2] and Fuchs[4] research groups have reported on improved pinning in zinc-doped Y123 single grains. Cu (2) sites from CuO_2 planes are substituted by zinc elements,[8] which induces local magnetic moments in these planes close to the zinc impurities.[9] The coupling of such moments with the conduction band causes an Abrikosov–Gorkov pair breaking and, consequently, a local superconductivity suppression.[10]

Even so, the Y123 bulk superconductors have been reported to regularly fracture during high field activation due to the stresses imparted by the flux density gradients.[2–4,11] The maximum stress that Y123 materials can withstand is governed by their fracture toughness $K_{1c} \propto \sigma_R \times \sqrt{a_0}$ which depends on the material strength σ_R and also the primitive size a_0 of the largest pore or crack produced during the single-domain superconductor processing. Indeed, when the Y123 material is heated to the temperature high above the peritectic decomposition one

Dr. D. Kenfaui, P.-F. Sibeud, Dr. X. Chaud
CNRS/CRETA – LNCMI, B.P. 166,
38042, Grenoble, Cedex 09, France
E-mail: driss.kenfaui@live.fr
E. Louradour
CTI SA, 382 du Moulinas-La Resclause,
30340, Salindres, France
Prof. J. G. Noudem
LUSAC/CRISMAT-CNRS UMR 6508, UCBN, rue Aragon,
50130, Cherbourg, France

DOI: 10.1002/adfm.201304083

during the TSMG processing, a large amount of oxygen gas was generated from the precursors such that: $YBa_2Cu_3O_{7-\delta}$ (Y123) → Y_2BaCuO_5 (Y211) + liquid + O_2. The sample readily loses oxygen and $7-\delta$ becomes ≈6.3, but some of the oxygen gas, in particular that located away from the external material surface, remains as bubbles in the crystal. The bubbles entrapment results hence in the formation of large number of micro-voids which are pores difficult to eliminate after crystal growth.[3,12]

The grown Y123 grain is, moreover, generally annealed at 400–500 °C under 0.1 MPa oxygen flow, a treatment, so-called conventional oxygenation, applied with a view to increasing oxygen content to $7-\delta > 6.8$,[13,14] thereby recovering the superconducting properties. However, Specht et al.[14] have observed that the crystalline cell c-parameter is constantly shortened when the Y123 material is cooled in air or oxygen to room temperature, and a tetragonal to orthorhombic transformation occurs around 500 °C. Since the *c*-parameter shrinks over a very short crystal depth imputable to the very low oxygen diffusion rate, 10^{-7} cm^2 s^{-1} in the (*a*,*b*) planes and still lower by 4–6 order of magnitude along the *c*-axis,[15,16] the external thin oxygenated layers are thus under a tensile stress since the crystal core is still much less oxygenated possessing the primitive *c*-parameter. The induced oxygen gradients and the crystallographic transformation consequently cause stresses exceeding the Y123 material strength σ_R (10–30 MPa),[17] which leads to an exhaustive cracking in (*a*,*b*) planes and in cleavage (*a*,*c*) and (*b*,*c*) ones as well.

Both pores and cracks dramatically impair not only the mechanical reliability but also the trapped field performances through a drastic reduce in the current loops size.

Besides these defects, the thermal conductivity of the Y123 material is anisotropic and depicts very low values: 14 and 3.5 W m^{-1} K^{-1} in the (*a*,*b*) planes and along the *c*-axis, respectively.[3] The heat generated in the Y123 bulk superconductor during the trapping field process cannot hence be transferred outside the material without harming the trapping properties or, even worse, causing a sudden thermal instability as flux jumping leading to the suppression of trapped field and irreversible damage of the material.[2–4,10,11]

Thus, a macroscopic cracking has been reported on a 26 mm-diameter zinc-doped Y123 single pellet limiting B_{max} on 4.4 T at 58 K. B_{max} was improved to 11.4 T at 17 K on a similar-sized sample processed from Y-Ba-Cu-O precursors with added 10 wt% Ag doping and encapsulated the pellet in a Cr-Ni steel ring to exert a compressive stress on Y123 material during the trapped field process. A larger B_{max} of 14.35 T was recorded at 22.5 K in the gap between two of such samples before being fractured.[4] Likewise, Tomita et al.[3] observed a large crack on two Y123 pellets of 26.5 mm in diameter previously wrapped in carbon fiber and impregnated with resin, limiting then B_{max} on 6 T at 31 K in the gap between them although an external magnetic activation as strong as 18 T was applied. They measured a record B_{max} value of over 17 T at 29 K between two Y123 samples after having inserted aluminum (Al) wire as a heat sink into their center, and impregnated them with Bi-Pb-Sn-Cd alloy.

As a result, the development of reliable Y123 superconductors required for a large-scale use has thus far been severely hindered, and their applications consequently remain confined to niche markets although their potential to generate extremely strong trapped fields.

Here we report a practical approach by which pore-free and crack-free Y123 large-grain superconductors endowed with promoted thermal exchange ability are economically fabricated with high a degree of reproducibility. The approach is based firstly on the growth of Y123 thin-wall single domains from drilled pellets to let the oxygen gas to be holly released when the Y-Ba-Cu-O precursors melt, and secondly on the progressive annealing at high temperature under oxygen pressure of the grown crystals to minimize the stresses deriving from the oxygen gradients by speeding up the oxygen diffusion. By virtue of large specific areas and reduced diffusion paths provided by the holes network, this oxygenation processing is effective as well as economical. The approach finely intends to greatly improve the thermal exchange by inserting metal wires possessing much larger thermal conductivity in the holes, and mechanically reinforce it through a resin/metal impregnation to avoid both temperature increase inside the crystal and material fracture during the trapping field process. A substantial effort has also gone into developing an experimental set-up enabling the measurement of the trapped field performances which were intensively investigated in 17–92 K temperature range and compared to the largest ones reported to date on large Y123 single-grain superconductors.

2. Fabrication of Large Thin-Wall $YBa_2Cu_3O_{7-\delta}$ Single Grains

Large thin-wall Y123 single domains were then grown from drilled pellets by using TSMG process described in the Experimental Section. The crystal growth was oriented by a commercial 2 mm × 2 mm seed, NdBCO thin layer deposited on MgO substrate (Theva Gmbh films), placed on the upper surface of the precursor preforms at room temperature before TSMG processing. The choice of such seed is based on the considerations that its crystallographic structure is similar to Y123 phase, its melting point higher and its composition chemically stable with the BaCuO liquid at elevated temperature in the peritectic decomposition sate of the sample, necessary properties to let the seed to act as a nucleation center promoting growth of large individual grain.[1] **Figure 1**a shows the top view morphology of as processed thin-wall single domain, wherein the crystal growth began beneath the seed at a temperature of about 1004 °C to spread across the whole of the disk surface. The sample depicts four growth facet lines as for the traditional plain single domains[1] and the square pattern with sides parallel to the a/b-axis, which suggests that the orientation of the Y123 single grain is similar to that of the seed one. The crystal growth proceeds to the edge of the preform along all its depth as seen in Figure 1b. The elaborated thin-wall crystals are cooled under a nitrogen flow from 930 °C to room temperature to prevent oxygen uptake causing cell parameters change, thereby avoiding material cracking.

It is relevant to note here that the NdBCO/MgO seed use is timesaving and yielded Y123 large single domains with higher degree of reproducibility compared with $NdBa_2Cu_3O_{7-\delta}$ or $SmBa_2Cu_3O_{7-\delta}$ small crystal slices often hardly cleaved along the a/b-axis from multi-grain samples to be used as seed.[1]

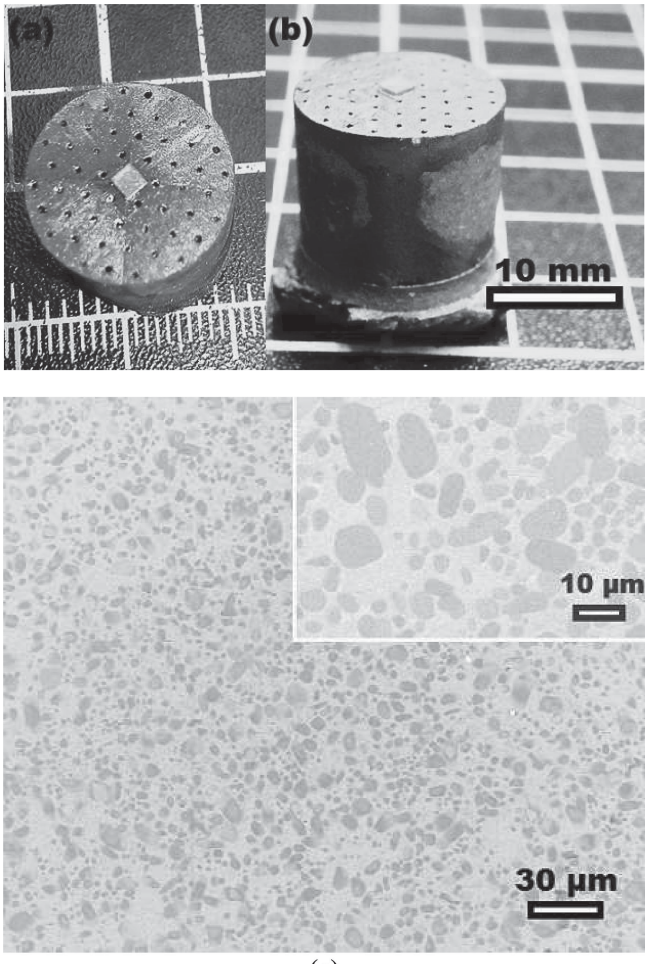

Figure 1. Thin-wall Y123 large grain grown from a drilled preform. a) Top and b) side view of an Y123 single grain. c) SEM image of mirror-polished surface parallel to the vertical *c*-axis of the single grain progressively oxygenated at 700 °C under 10 MPa for 12 h: Y123 matrix comprises small Y211 particles. The micrograph particularly shows the absence of pores and cracks in the microstructure even at high magnification (inset).

The holes network of the sample does not hinder the crystal growth and is not disturbed after TSMG processing, but the pellet diameter macroscopically shrinks from 20 to 15.9 ± 0.2 mm, inducing a reduction of the holes diameter from 0.5 to 0.41 ± 0.01 mm and the walls thickness from 2.5 to 2.07 ± 0.05 mm.

3. Progressive Oxygenation at High Temperature Under Pressure

To recover the superconducting properties, the processed thin-wall Y123 single domains underwent an amended annealing treatment, so-called progressive oxygenation,[18] in an effort to diminish, or even prevent, crystal cracking. Effectively, the progressive oxygenation aims to maintain the stresses induced by the oxygen gradients at levels below the Y123 material strength. A full oxygenation has already reported for bars,[18] cut from a Y123 single domain with a ≈1.5 mm-thickness parallel to the (*a*,*b*) planes, annealed by using such treatment. It is, therefore, clear that large thin-wall Y123 single domains are well-suited for being progressively oxygenated. The holes network bestows them with large specific areas and considerably reduced diffusion paths. Whatever the size of the thin-wall sample, the crystal depth that matters for oxygen diffusion is hence the wall thickness and is no longer the pellet diameter as for the traditional plain single domains.[1–6,10,11] However, achieving a full oxygenation for thin-wall single domains, by applying the progressive annealing with a final dwell at 400–500 °C, shall be very time-consuming (≈ 30 days) due to the low oxygen diffusion into the Y123 crystal at this temperature range.[18] That will be a major limitation of large-scale Y123 bulk superconductor applications. We have found the way to cope with this challenge through the speeding up of the oxygenation of thin-wall Y123 single domains by applying the progressive annealing at higher temperature, and under high oxygen pressure to simultaneously compensate for subsequent lower oxygen content in this temperature range and enhance the oxygen diffusion rate by displacing the oxygen-temperature equilibrium toward the higher temperatures.[13,19–21] We have first determined the experimental conditions enabling to reach the optimized trapped field at 77 K.[21] The processed thin-wall Y123 single domains were thus progressively oxygenated under these conditions of 700 °C and 10 MPa oxygen pressure for 12 h in a classical tubular furnace comprising a vessel resisting oxidization at high temperature under pressure up to 16 MPa.[21,22] The temperature and pressure cycles were applied and the atmosphere controlled such that: the furnace air is primarily substituted by the nitrogen gas at 30 °C. The temperature is then constantly raised to 900 °C at a rate of 60 °C h^{-1} under a flowing atmosphere (0.1 MPa), which was progressively changed from 100% nitrogen to 100% oxygen by using a program[18] aiming to maintain the oxygen content at about $7 - \delta = 6.3$ in the Y123 crystal.[13,20,21] A half-hour later, the sample was cooled to the dwell temperature of 700 °C at 10 °C h^{-1}, while the oxygen pressure was introduced into the furnace at 850 °C with rates of 0.2 MPa h^{-1} from 0.2 to 3 MPa and 1 MPa h^{-1} from 3 to 10 MPa. The pressure is finely maintained for 12 h at 700 °C. The total time, spent here to fully oxygenate the thin-wall Y123 samples, does not exceed 3 days, which is less long by more one order of magnitude compared to the conventional oxygenation (30 days) used so far for the traditional plain samples.[1–4,10,11] That makes clear the outstanding time and energy savings brought by the approach taken here, which would launch the widespread use of Y123 bulk superconductors for the aforementioned applications.

4. Microstructure

Scanning electron microscopy (SEM) observations of mirror-polished surface (Figure 1c) **containing** the vertical c-axis of the thin-wall single domain progressively oxygenated exhibit typical complex microstructure features known from melt-textured processed Y123 bulk materials. The Y123 matrix, in bright contrast, comprises Y211 particles which are uniformly distributed and can be categorized into two types of size: small majority inclusions with a size spanning from 1

to 4 μm, and large minority particles that can reach 18 μm in length. The Y211 particles size is generally larger than that reported elsewhere,[22] perhaps due to the initial Y211 precursor since the single domains were prepared by using the same process.

It should be noted that the SEM observations were performed on several cross-sections obtained by catting the single domain in the direction parallel to its vertical c-axis. For each cross-section, the cutting was carried out at a different distance from the center of the sample disk. After mirror polishing, the SEM investigations were thoroughly done along all the surface of each cross-section.

These observations, on the other hand, showed the absence of pores, which suggests that the holes network permitted the oxygen gas to be completely released during the precursors melting at high temperature. The oxygen bubbles crossed much more readily thin walls of the crystal to get out through the large specific areas than a pellet diameter in the case of the traditional plain samples reported heretofore.[1,3,4,10–12] That enables to avoid the formation of micro-voids, resulting in a pore-free microstructure of the thin-wall single domain.

We can see likewise a crack-free microstructure of this sample, even at higher magnification as shown from the inset of Figure 1c, reflecting a marked reduction in stresses tied to oxygen gradients due to speeding up the oxygen diffusion in the Y123 crystal by using the progressive annealing at high temperature under oxygen pressure. We further believe that the stresses derived from the thermal gradients, in particular those induced in the Y123 material during crystal growth or oxygenation annealing owing to its low anisotropic thermal conductivity, were diminished as well thanks to the high thermal exchange allowed by the large specific areas. The stresses ultimately dropped below the Y123 material strength allowing the avoidance of crystal cracking.

Several mirror surfaces parallel to the (*a*,*b*) planes were also obtained by cutting (and then polishing) several ≈ 2 mm-diameter disks from another single domain prepared in the same conditions. This time the cutting was done in the direction perpendicular to the c-axis of this single domain. Likewise, the SEM observations revealed no pores and no cracks on the surfaces of these disks, confirming then the absence of these default inside the sample.

Figure 1c shows the pore-free and crack-free microstructure of a center zone of cross-section cut from the core of the single domain.

5. Mechanical Reliability

To assess the mechanical reliability of a thin-wall sample progressively oxygenated, Vickers indentation tests were performed in ambient air to nucleate radial cracks at the corners of the imprints introduced on polished surfaces. The cracks emanating from the corners of a Vickers imprint (**Figure 2**) are stopped when the residual stress driving force at the crack tip is in equilibrium with the fracture toughness, K_{Ic}, of the material. By measuring crack lengths c_1 and c_2 and using the formula reported elsewhere,[23–25] the imprints on the (*a*,*b*) and (*a*,*c*)/(*b*,*c*) planes yield mean K_{Ic} values of 2.88 ± 0.09 and 3.1 ± 0.21 MPa $m^{1/2}$, which is the highest values reported hitherto for the Y123 material without added Ag doping. Indeed, they are larger by factors ranging from 1.51 to 1.94 and from 1.47 to 2.07 than the K_{Ic} values reported on (*a*,*b*)[26–28] and (*a*,*c*)/(*b*,*c*)[26,29,30] planes of the plain Y123 single domains conventionally oxygenated, respectively, which is predominantly ascribed to the pore-free and crack-free microstructure of the thin-wall sample.

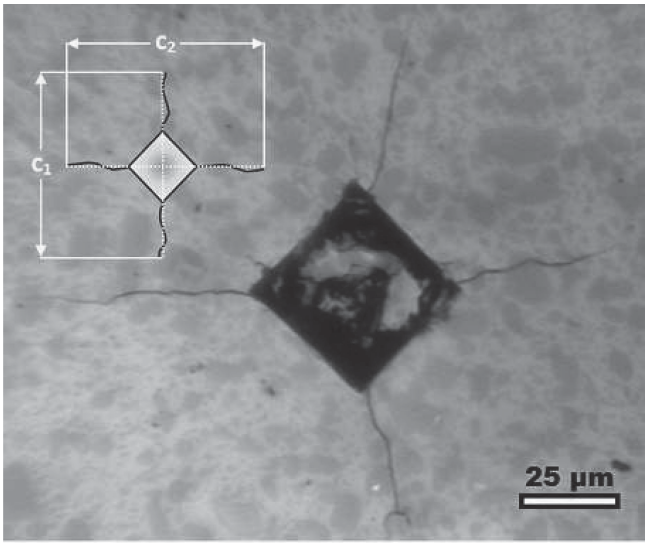

Figure 2. Optical micrograph showing a Vickers indentation introduced on a polished section of a thin-wall single grain progressively oxygenated to nucleate radial cracks at the corners of the imprint for determining fracture toughness.

The achieved toughness in (*a*,*b*) planes shows furthermore an increase by a factor spanning from 1.02 to 1.51 compared to the values published in an equivalent direction for single domains processed from Y-Ba-Cu-O precursors to which 5–15 wt% Ag particles (12 μm) were added.[27,28,31] However, it remains lower by 0.52 MPa $m^{1/2}$ than the value reported for an Y123 single-domain sample in which are uniformly distributed 15 wt% Ag finer particles (2 μm).[28] It is to be noted that if the addition of silver was used to improve the fracture toughness of the plain Y123 samples, it was reported nonetheless to impair their trapped field capabilities.[2,4,11]

The fracture toughness was otherwise reported to drop for the plain Y123 samples with decreasing the temperature[32] and increasing thermal cycles as well,[30] due to the evolution of cracks introduced during the material processing. This problem would be significantly limited in the thin-wall domains since the pores and cracks were avoided.

6. Trapped-Field Performances

The thin-wall Y123 superconductor was characterized by measuring the trapped-field profile at 77 K by cooling the sample into the liquid nitrogen bath in an applied field of 1.5 T provided by a superconducting coil. After switching off the external field, the remnant induction at the upper surface of the sample was measured using an axial Hall sensor. The scan is made at a distance of 0.2 mm from the surface with a grid step of

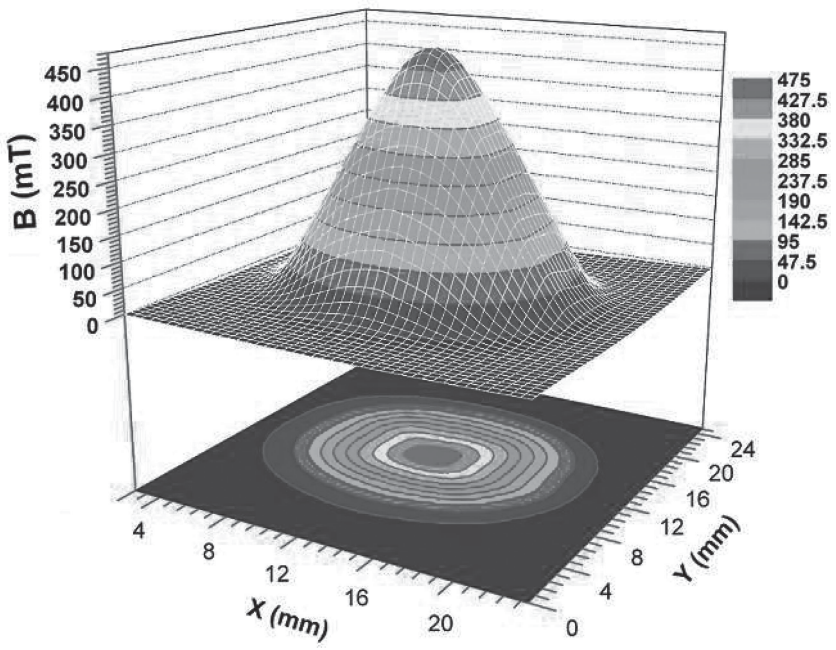

Figure 3. Flux mapping results obtained for the thin-wall single grain progressively oxygenated. Top: Trapped-field spatial distribution at 77 K depicting a single homogeneous peak culminating at B_{max} of 0.475 T. Bottom: The corresponding 2D representation of the surface induction evidencing the persistent currents freely flow in large undeformed loops at the scale of the (*a*,*b*) planes of the single grain.

0.5 mm. The obtained profile (**Figure 3**, top) reveals a typical shape of the trapped-field spatial distribution in Y123 bulk superconductors with a single homogeneous peak elucidating the single-domain quality of the sample, in keeping with the macroscopic observations (Figure 1). The persistent currents are almost entirely unimpeded and, hence, freely circulate in large undeformed loops at the scale of the (*a*,*b*) planes of the thin-wall single grain as evidenced from the trapped field 2D representation (Figure 3, bottom). That is fostered by the achieved pore-free and crack-free microstructure as well as the absence of residual grains, thereby emphasizing the relevance of the approach taken here. It resulted then in a maximum trapped field B_{max} of 0.475 T at 77 K at the surface center of ≈16 mm-diameter thin-wall pellet, which is more than 2.3 fold a similar-sized Y123 plain sample reported elsewhere,[1] and even comparable to SmBCO single domains with a similar size as well,[1] materials considered so far to trap larger fields than those by Y123 ones.[1] The obtained B_{max} on the thin-wall single domain yields a trapped field density $B_{max}/s = 0.24\,\mathrm{T\,cm^{-2}}$ (*s* is the disk surface of the sample ≈1.99 cm^2), which is larger by factors of 2.9 and 1.8 than the values attained by Gruss et al.[2] (0.083 T cm^{-2}) and Tomita et al.[3] (0.13 T cm^{-2}) on 35 and 26 mm-diameter Y123 single domains trapping B_{max} of 0.8 and 0.7 T, respectively. It likewise at less two times higher than the values achieved by Fuchs et al.[4] (0.11 T cm^{-2}) and Gruss et al.[2] (0.125 T cm^{-2}) on a 35 mm-diameter zinc-doped Y123 single domains giving B_{max} of 1.04 and 1.2 T, respectively. That highlights more clearly the much larger size of the persistent current loops flowing in the (*a*,*b*) planes of the thin-wall single domain as result of the achieved pore-free and crack-free microstructure.

Since the trapped field substantially increases with decreasing temperature, we have developed an experimental set-up at CRETA laboratory of Grenoble enabling to measure the temperature dependence of the maximum trapped field B_{max} in the 17–92 K range. The system is consisted of a sample stage cooled by the instrumented Cryomech AL230 cryocooler in a cryostat inserted in an Oxford superconducting coil providing an external magnetic field up to 7 T. By wrapping the cryocooler in a superinsulation film (JEHIER SA – HUTCHINSON Group, France) as shown in **Figure 4**a and creating a vacuum of about 10^{-4} mBar in the cryostat, the sample stage was cooled from room temperature to <20 K in 30 min, which represents a realistic solution to the cooling problem in terms of not only the time but also the cost.

Thus, we first used this set-up to calibrate Hall and Cernox sensors in (0–7 T/11–100 K) temperature and field ranges.

To investigate its trapping capabilities, the thin-wall superconductor was mounted in a copper support fixed on the cold-head of the cryocooler (Figure 4a), and a Hall sensor was located at the central position on its upper surface (Figure 4b). A Cernox sensor was placed in the immediate vicinity of it to monitor the sample temperature. The sample as well as both sensors was mechanically fixed as shown in Figure 4c to concomitantly deal with magnetic forces induced upon the trapping field and insure good thermal contacts.

For all the tests, the thin-wall single domain was first cooled to 100 K and maintained at this temperature, which is above the critical one of Y123 superconductor, while the external field was increased up to 7 T. The sample was then cooled to the measuring temperature. When thermal equilibrium was attained, the temperature of the cold-head of the cryocooler was lower by ≈1.5 K because of the thermal resistance in the interfaces cryocooler head–copper support–sample and the low thermal conductivity of Y123 material. The trapped field and temperature of the sample were continuously recorded in steps of 1 s whilst the external field was swept down to zero at a rate of 0.1 T min^{-1} to avoid thermally induced flux jumps.[2–4,10,11]

Figure 4d shows the time dependence of the trapped field measured at the center on the top of the thin-wall Y123 single domain during tests where a different measuring temperature was selected for each one. The measurements were performed while the applied field was ramped down from 7 T to zero. For each measuring temperature, the field on the single-grain superconductor gradually decreased and remained at a corresponding B_{max} when the external magnetization was at zero. The lower the measuring temperature, the higher the trapped fields B_{max}, owing to stronger pinning force. A maximum trapped field B_{max} of 5.2 T was achieved at 17 K, which is suggestive of an extremely strong flux pinning force although no doping was used.[4,10,11] The corresponding trapped field density $B_{max}/s = 2.62\,\mathrm{T\,cm^{-2}}$ is distinctly larger than the value

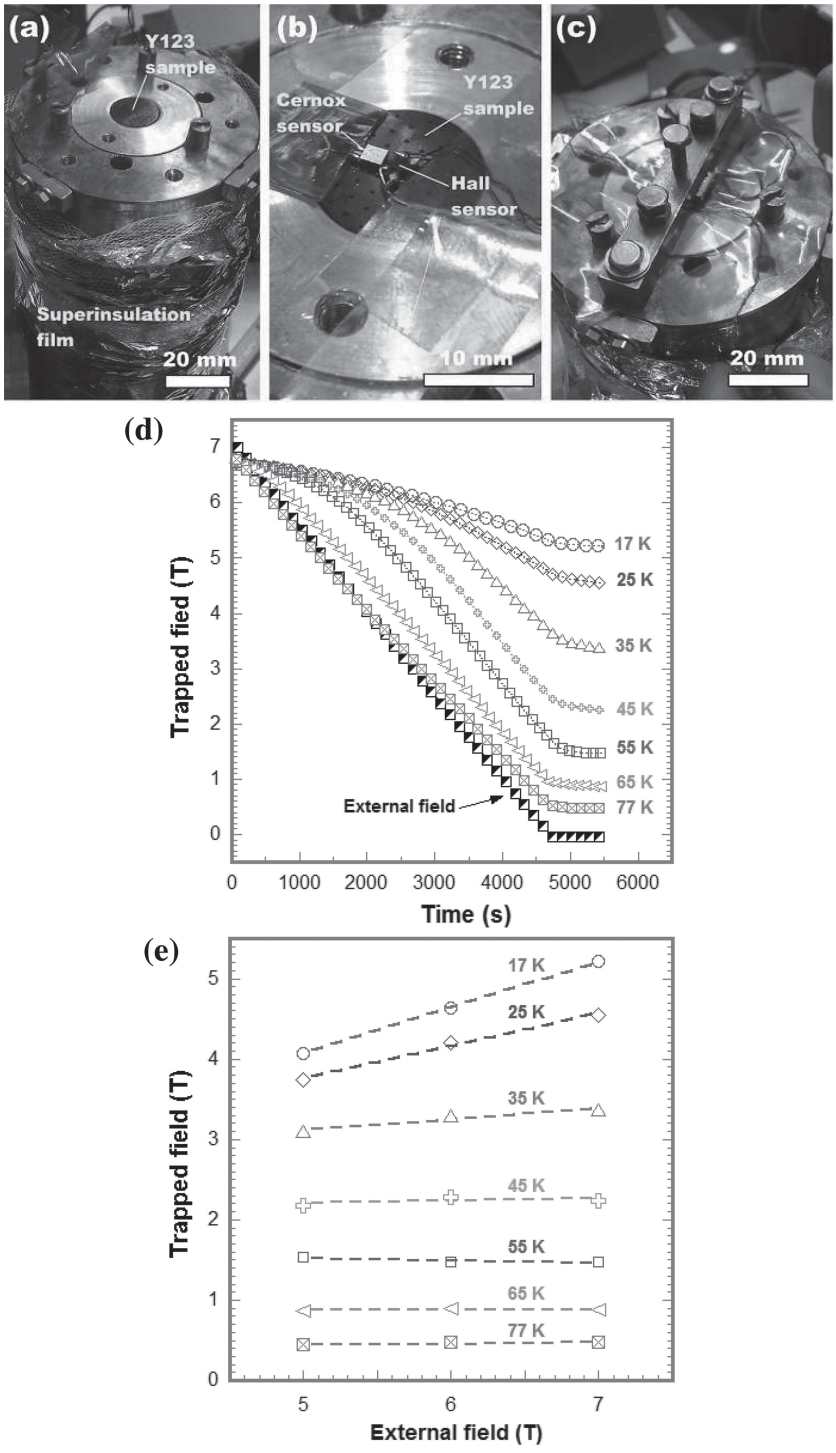

Figure 4. The trapped field measurements on the unreinforced thin-wall superconductor at selected measuring temperatures in the 17–77 K range. a) An Y123 thin-wall sample mounted in a copper support fixed on the cold-head of the cryocooler wrapped in a superinsulation film. b) A Hall sensor located at the central position on the upper surface of the sample, and a Cernox sensor placed in the immediate vicinity of it. c) Mechanical fixture of the sample and the sensors. d) The time dependence of the maximum trapped field B_{max} measured at the center of the thin-wall Y123 superconductor for different selected measuring temperatures while the applied field decreased from 7 T to zero. The external field was plotted as well. e) The trapped field B_{max}, recorded at different measuring temperatures after the external magnetization was removed, as a function of the nominal applied field.

(2.15 T cm^{-2}) attained at the same temperature by Fuchs et al.[4] on a 26 mm-diameter Y123 single plain sample, processed from Y-Ba-Cu-O precursors with added 10 wt% Ag doping and reinforced by steel ring, trapping B_{max} up to 11.4 T. This result is more reflective of much larger size of the persistent current loops flowing in the (*a*,*b*) planes of the thin-wall single grain.

Two similar test batches were thereafter conducted on the same sample by applying the respective external fields of 6 and 5 T. The trapped field was likewise monitored during sweeping down the external field. In Figure 4e, the maximum trapped field B_{max}, recorded at different measuring temperatures after the external magnetization was removed, is depicted as a function of the nominal applied field. Whereas the field B_{max} trapped at 77, 65 and 55 K reveals saturation trend, it linearly enhances at lower temperatures in the investigated external field range, and the B_{max} increase becomes steeper as the measuring temperature is lower. It suggests that the thin-wall sample possesses the potential to trap stronger field than 5.2 T if a higher external field is applied for magnetic activation.

On the other hand, it has to be noted that the maximum trapped field at a selected measuring temperature is very sensitive to the temperature evolution inside the sample during the trapping process. Indeed, even in a case where no flux jumping occurs, a temperature increase into the plain sample was reported as result of a heat generated by dissipative flux motion during ramping down the applied field.[2,11] Such heat cannot be rapidly dissipated because of the very low thermal conductivity of the Y123 material, which releases a part of the magnetic energy stored in the Y123 superconductor.

In the case of the thin-wall superconductor, nor is the generated heat immediately transferred outside the sample through the larger specific areas because of the vacuum applied in the cryostat that is the same into the holes of the sample, which would have caused lose of a part of the trapped field.

The cooling of the thin-wall sample is ensured through the lateral surface and, in particular, the bottom surface which is in contact with the holder.

To foster the thermal exchange in the interior regions of the sample, we inserted then 0.3 mm diameter Al wires, of a much larger thermal conductivity (≈4530, 3450, and 2150 W m^{-1} K^{-1} at 17, 25, and 35 K, respectively), into the holes. The sample was

thereafter impregnated with a mixture of resin[3] and 4 wt% Al metal inclusions; as Al metal has an expansion coefficient (2.3×10^{-5} K^{-1}) closer to that of Y123 (1×10^{-5} K^{-1}) than that of the resin ($3–4 \times 10^{-5}$ K^{-1}), which may avoid damage in the resin during the cooling cycles. The higher thermal conductivity of Al metal inclusions could improve that of the mixture. The impregnation was carried out in vacuum to avoid any formation of the oxygen gas micro-voids into the resin.[3] The reinforced sample was then mirror-polished on its two faces to remove the surface resin (**Figure 5**a).

Figure 5b shows the time dependence of the temperature and trapped field measured at the center on the top of the reinforced sample for selected measuring temperatures of 17, 25, and 35 K while the applied field was ramped down from 7 T to zero at a sweep rate of 0.1 T min^{-1}. To ease a comparison with the unreinforced thin-wall superconductor, the curves corresponding to this latter were plotted as well. The trapped fields for the reinforced superconductor are patently shifted to higher values, reflecting a noteworthy fostering of the thermal exchange into the sample. The heat generated during the trapping process is instantly transferred to the sample holder by means of Al wires thanks to their much larger thermal conductivity, thereby safeguarding the magnetic energy stored in the thin-wall Y123 superconductor. Since Al wires were inserted into all the holes network of the pellet, the internal thermal exchange is hence more uniform than that achieved by Tomita et al.[3] and its promotion consequently better.

It should be further noted that the achieved encapsulating of the sample in the mixture resin /Al inclusions as shown in Figure 5a generates compressive stresses during cooling due the larger thermal expansion coefficient of this mixture compared to that of the Y123 sample in its (*a*,*b*) planes. Such stresses compensates for those induced by the gradient of the trapped field in the single-grain sample.

The reinforced thin-wall superconductor traps hence maximum fields B_{max} = 4.5 T at 35 K similar to the value recorded on the unreinforced one at 25 K, and even 5.49 T at 25 K larger than that trapped on the latter at 17 K.

A maximum B_{max} value of 6.34 T was achieved at 17 K, representing an enhancement of more than 21% compared to the unreinforced sample. Such B_{max} value leads to an outstanding field density $B_{max}/s = 3.19\,T\,cm^{-2}$, which is among the highest values achieved so far for Y123 single-domain materials, including doped and/or reinforced ones. This result testifies for a dramatic increase in the size of the persistent current loops combined to a considerable promotion of the internal thermal exchange in the reinforced thin-wall Y123 superconductor and to a compensation for induced magnetic stresses.

After measuring B_{max} when the external magnetization was entirely removed, the samples were heated up to >92 K for each test in order to remove the remanent field. To prevent eventual thermally induced flux jumps, the heating rates were set at 0.2 K min^{-1} from 17 to 35 K and higher from 35 to >92 K. The trapped field and temperature were continuously monitored. In **Figure 6**a, shown is the temperature dependence of the maximum trapped field B_{max} for the unreinforced and reinforced thin-wall Y123 superconductors. Both samples behave in a similar way, that is, their $B_{max}(T)$ curves show a strong increase of the trapped field with decreasing temperature. The

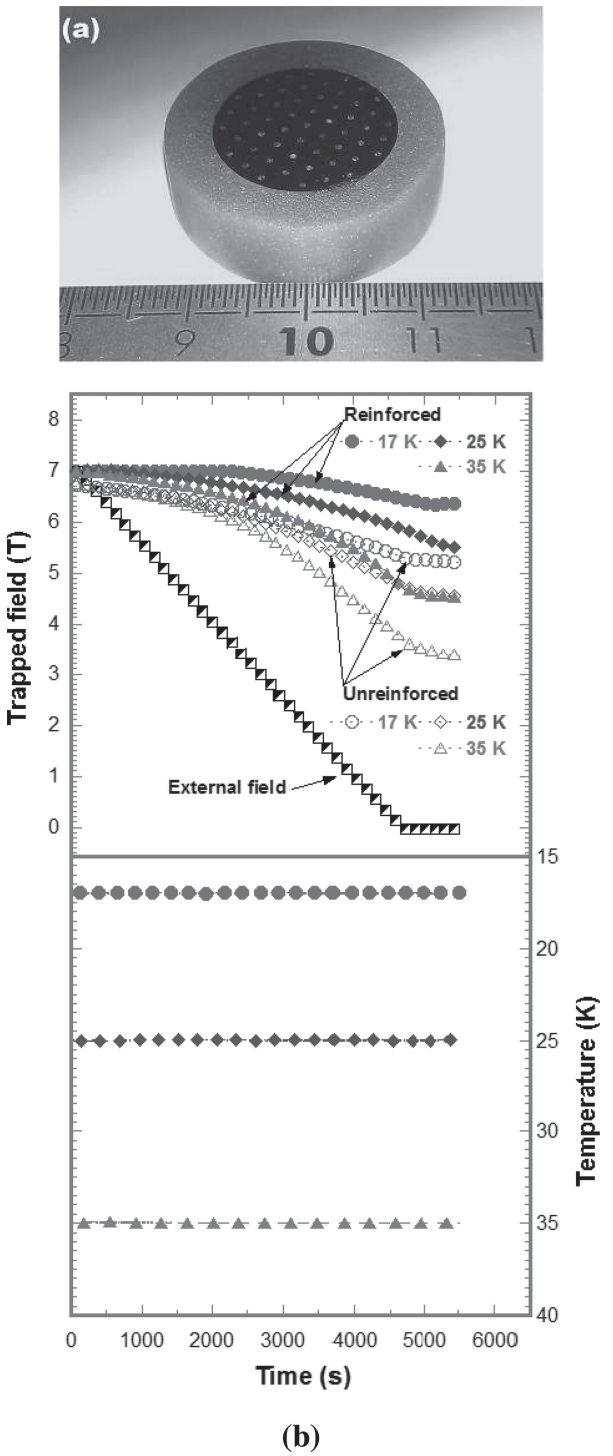

Figure 5. The trapped field measurements on the reinforced thin-wall superconductor at measuring temperatures of 17, 25 and 35 K. a) The thin-wall superconductor reinforced by inserting Al wires in the holes and an impregnation with resin loaded in Al inclusions. Al inclusions in the resin are visible to the naked eye. b) The time dependence of the temperature and maximum trapped field B_{max} measured at the center on the top of the reinforced sample for selected measuring temperatures of 17, 25, and 35 K while the applied field was ramped down from 7 T to zero. To ease a comparison, the curves corresponding to the unreinforced thin-wall sample were plotted as well.

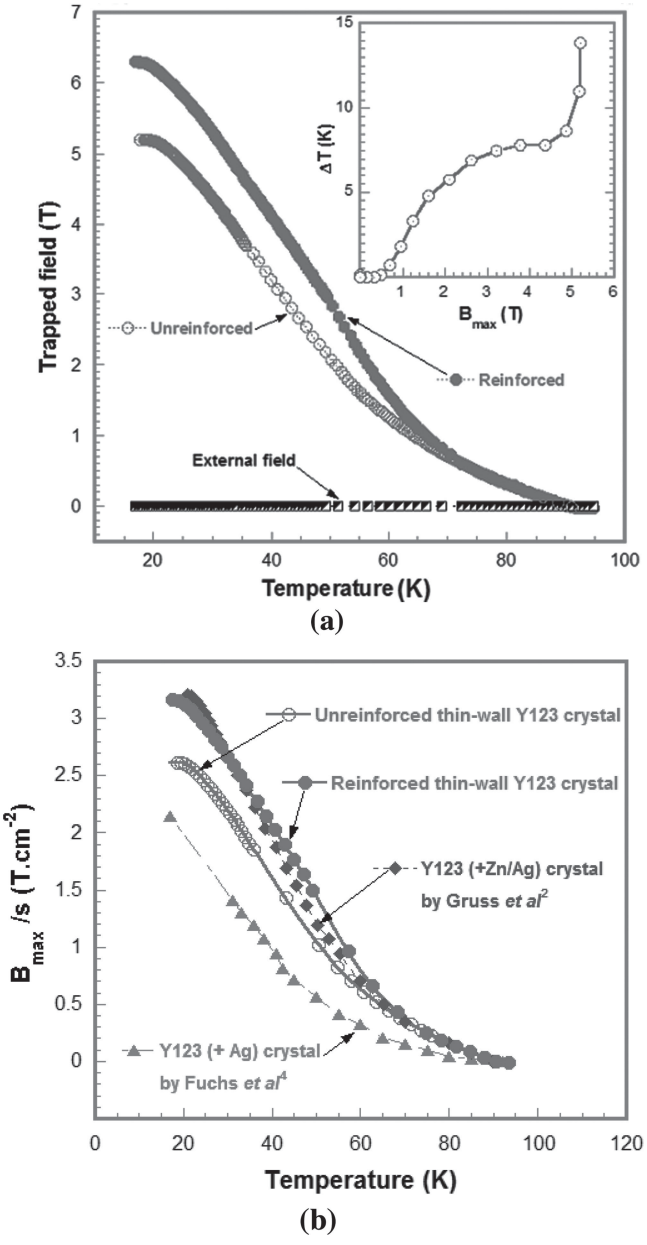

Figure 6. The temperature dependence of the trapped field performances in the 17–92 K range. a) The temperature dependence of the maximum trapped field B_{max} for the unreinforced and reinforced thin-wall Y123 superconductors during heating from 17 to 92 K. Inset: the temperature shift ΔT as function of the field B_{max} trapped by the unreinforced superconductor. b) The temperature dependence of the trapped field density B_{max}/s for the unreinforced and reinforced thin-wall Y123 superconductors compared to that of the strongest trapped field reported so far on reinforced Y123 and zinc-doped Y123 single disks (of 26[4] and 22 mm[2] in diameter, respectively) with 10 wt% Ag and embedding in a steel tube.

fostering of the thermal exchange into the reinforced superconductor associated with the compensation for induced magnetic stresses resulted in a considerable shift of $B_{max}(T)$ to higher temperature. The B_{max} value of 5.2 T recorded on the unreinforced superconductor at 17 K is attained on the reinforced one at 31 K, representing a temperature shift of $\Delta T = 14$ K. The temperature shift ΔT increases with the maximum field B_{max} trapped by the unreinforced sample as can be seen from the inset of Figure 6a. That means that ΔT rises with decreasing temperature, which can be ascribed to larger heat, produced by higher flux motion into the crystal at lower temperatures, dissipated thanks to higher thermal conductivity of Al wires.

In Figure 6b, the temperature dependence of the trapped field density B_{max}/s for the unreinforced and reinforced thin-wall Y123 superconductors are plotted with that of the strongest trapped field reported so far on Y123 single disks. Compared with the 26 mm-diameter plain Y123 sample reinforced by adding 10 wt% Ag and embedding in Cr-Ni steel tube, reported by Fuchs et al.[4] to trap a field as strong as 11.4 T at 17 K, the B_{max}/s values of the thin-wall superconductors are shifted to higher trapped field densities, which is mainly derived from the larger size of the persistent current loops. The fostering of the thermal exchange in the reinforced thin-wall sample and the compensation for induced magnetic stresses boosted B_{max}/s to values larger, particularly in the 30–92 K temperature range, than those achieved by Gruss et al.[2] on 22 mm-diameter plain 0.12 wt% Zn doped Y123 single domain consolidated by 10 wt% Ag addition and encapsulating it into Cr-Ni steel ring, possessing the strongest volume pinning force and displaying the largest trapped field reported to date for a single sample (12.2 T at 22 K). It should be noted that the reported samples cited here were energized by a field as strong as 18 T.

Such results associated with the achieved high mechanical reliability outline the potential of the thin-wall superconductors to trap much stronger fields if higher applied field is available, which endorses the effectiveness of the approach taken here to develop high-performance and reliable Y123 single-domain superconductors.

7. Conclusions

Large thin-wall Y123 pore-free single grains were fabricated with a high degree of reproducibility. Compared to plain Y123 materials reported hitherto, the obtained samples were fully oxygenated in time less long by more one order of magnitude and the material cracking was avoided. The achieved pore-free and crack-free microstructure fostered enhanced fracture toughness and large size persistent currents, which stimulated the mechanical reliability and the trapped field performances. A considerable fostering of the internal thermal exchange and a compensation for induced magnetic stresses were achieved by inserting Al wires in the holes and impregnating the sample with resin loaded in Al powder, which leads trapped fields to shift to higher values. The B_{max} value of 5.2 T recorded on the unreinforced thin-wall superconductor at 17 K is attained on the reinforced one at 31 K. A maximum trapped field B_{max} of 6.34 T was reached at 17 K on ≈16 mm-diameter reinforced thin-wall superconductor, resulting in a striking field density $B_{max}/s = 3.19\ \mathrm{T\,cm^{-2}}$, which is among the highest values attained so far for Y123 materials.

It is clear from the results reported here that the proposed approach brings decisive solutions to many problems having impeded heretofore the development of bulk RE-Ba-Cu-O

single domains, which ushers in broad-based RE-Ba-Cu-O bulk superconductor engineering applications.

8. Experimental Section

Drilled Preform Preparation: The starting precursors 70 wt% Y123, 30 wt% Y211 and 0.15 wt% PtO_2 (in excess) were weighed and mixed in dry conditions inside an argon-filled glove-box with less than 0.5 ppm O_2 and H_2O. The powder mixture was uniaxially cold-pressed under moderate pressure (4.5 MPa) into drilled pellets using 20 mm-diameter die with 0.5 mm-diameter embedded needles enabling to introduce a regular network of holes spaced by 2.5 mm-thickness walls.

$YBa_2Cu_3O_{7-\delta}$ Crystal Growth: The prepared drilled preforms were put on an alumina-bearing plate with two intermediate buffer layers: a layer of Y_2O_3 powder to absorb liquid loss and prevent reaction with alumina, and a 2 mm-thickness disc of {80 wt% Y123 + 20 wt% $YbBa_2Cu_3O_{7-\delta}$} mixture to avoid the nucleation of parasite crystals from the pellet bottom through the introduction of elements possessing lower melting point. A commercial seed with dimensions of 2 mm × 2 mm, cut out Theva Gmbh films (a 200 nm-NdBCO thin layer deposited on MgO substrate), was placed at the central position on top of each preform with the (*a*,*b*) plane of the NdBCO film in direct contact with the surface precursor preform. The entire arrangement was placed in a box furnace equipped with in-situ video monitoring which allows real-time control of the crystal growth. The samples were rapidly heated in air to 1054 °C, held for 2 h to get complete peritectic decomposition into a liquid rich in barium and copper, and skeleton of solid Y211 inclusions. They were quickly cooled to 1020 °C before setting cooling at very low rates (<2 °C h^{-1}). The crystal growth starts around 1004 °C in a narrow solidification window where the samples are gently cooled (0.1 °C h^{-1}) till the growth gets at the preform edge. The growth proceeds down to the samples bottom with a slight faster cooling (0.5–1 °C h^{-1}). The single-grains are finely cooled under a nitrogen flow from 930 °C to room temperature.

Assessment of the Fracture Toughness: Using a MTS-BRUCK mechanical testing device, a course of Vickers indentation tests at room temperature were carried out on polished sections of a thin-wall sample progressively oxygenated. The indentation induces micro-cracking around the indent impression as shown on the micrograph of Figure 2. The fracture toughness, K_{Ic}, was computed from the applied load and the crack lengths c_1 and c_2 according to the formula reported elsewhere.[23–25] The loading time was set at 10 s and the imprints were introduced in the (*a*,*b*) and (*a*,*c*)/(*b*,*c*) planes. At least 15 valid imprints were performed at each direction to assess the mean K_{Ic}.

Acknowledgments

This work is supported by the French National Research Agency (Agence Nationale de la Recherche – ANR) through the grants ANR-09-MAPR-002 (ASPAMEX Project) and ANR-2010-BLAN-0944–02 (REIMS project). The authors thank Dr. Alain Ravex for the shrewd advice on cryogenics, and Dr. Moussa Gomina and Dr. Daniel Bourgault for the fruitful discussions on mechanical and magnetic properties.

Received: December 5, 2013
Revised: February 5, 2014
Published online: March 24, 2014

[1] N. H. Babu, Y. Shi, K. Iida, D. A. Cadrwell, *Nat. Mater.* **2005**, *4*, 476–480.
[2] S. Gruss, G. Fuchs, G. Krabbes, P. Verges, G. Stöver, K.-H. Müller, J. Fink, L. Schultz, *Appl. Phys Lett.* **2001**, *79*, 3131.
[3] M. Tomita, M. Murakami, *Nature* **2003**, *421*, 517–520.
[4] G. Fuchs, P. Schatzle, G. Krabbes, S. Gruß, P. Verges, K.-H. Muller, J. Fink, L. Schultz, *Appl. Phys. Lett.* **2000**, *76*, 2107–2109.
[5] Y. Ren, J. Liu, R. Weinstein, I. G. Chen, D. Parks, J. Xu, V. Obot, C. Foster, *J. Appl. Phys.* **1993**, *74*, 718–719.
[6] M. Morita, K. Magashima, S. Takebayashi, M. Murakami, M. Sawamura, *Mater. Sci. Eng. B* **1998**, *53*, 159–163.
[7] C. P. Bean, *Phys. Rev. Lett.* **1962**, *8*, 250.
[8] C. Y. Yang, A. R. Moodenbaugh, Y. L. Wang, Y. Xu, S. M. Heald, D. O. Welch, D. A. Fischer, J. E. Penner-Hahn, *Phys. Rev. B* **1990**, *42*, 2231–2224.
[9] D. Poilblanc, D. J. Scalapino, W. Hanke, *Phys. Rev. Lett.* **1994**, *72*, 884–887.
[10] G. Krabbes, G. Fuchs, P. Schatzle, S. Gruß, J. W. Park, F. Hardinghaus, G. Stover, R. Hayn, S.-L. Drechsler, T. Fahr, *Physica C* **2000**, *330*, 18.
[11] G. Fuchs, G. Krabbes, P. Schatzle, S. Gruß, P. Verges, K.-H. Muller, J. Fink, L. Schultz, H. Eschrig, *Phys. B* **2001**, *294–295*, 398–401.
[12] N. Sakai, D. Ishihara, I. Inoue, M. Murakami, *Supercond. Sci. Technol.* **2002**, *15*, 698–701.
[13] H. M. O'Bryan, P. K. Gallagher, R. A. Laudise, A. J. Caporaso, R. C. Sherwood, *J. Am. Ceram. Soc.* **1989**, *72*, 1298–1300.
[14] E. D. Specht et al., *Phys. Rev. B* **1988**, *37*, 7426–7434.
[15] M. Klaser, J. Kaiser, F. Stock, G. Muller-Vogt, A. Erb, *Phys. C* **1998**, *306*, 188–198.
[16] S. J. Rothman, J. L. Routbort, U. Welp, J. E. Baker, *Phys. Rev. B* **1991**, *44*, 2326–2333.
[17] N. Sakai, S. J. Seo, K. Inoue, T. Miyamoto, M. Murakami, *in Advances in Superconductivity XI*, (Eds: N. Koshizuka, S. Tajima), Springer, Tokyo **1999**, 685–688.
[18] D. Isfort, X. Chaud, R. Tournier, G. Kapelski, *Phys. C* **2003**, *390*, 341–355.
[19] J. Karpinski, E. Kladis, *Nature* **1988**, *331*, 242–245.
[20] P. K. Gallagher, *Adv. Ceram. Mater.* **1987**, *2* [3B], 632–639.
[21] D. Kenfaui, X. Chaud, X. Hai, E. Louradour, J. G. Noudem, *IEEE trans. Appl. Supercond.* **2013**, *23*, 7201005.
[22] X. Chaud, J. Noudem, T. Prikhna, Y. Savchuk, E. Haanappel, P. Diko, C. P. Zhang. *Phys. C* **2009**, *469*, 1200–1206.
[23] J. B. Wachtman, *Mechanical Properties of Ceramics,* John Wiley and Sons, New York **1996**.
[24] A. P. Paker, *The Mechanics of Fracture and Fatigue, An Introduction*, E&F N Spon, London **1981**.
[25] F. Tancret, I. Monot, F. Osterstock, *Mater. Sci. Eng. A* **2001**, *298*, 268–283.
[26] Y. Feng, K. W. White, R. Meng, *Phys. C* **1997**, *276*, 295.
[27] H. Fujimoto, M. Murakami, N. Koshizuka, *Phys. C* **1992**, *203*, 103.
[28] A. Leenders, M. Ullrich, H. C. Freyhardt, *Phys. C* **1997**, *279*, 173.
[29] P. Schätzle, G. Krabbes, S. Gruss, G. Fuchs, *IEEE Trans. Appl. Supercond.* **1999**, *9*, 2022.
[30] J. Joo, S.-B. Jung, W. Nah, J.-Y. Kim, T. S. Kim, *Cryogenics* **1999**, *39*, 107.
[31] T. Okudera, A. Murakami, K. Katagiri, K. Kasaba, Y. Shoji, K. Noto, N. Sakai, M. Muratami, *Phys. C* **2003**, *392–396*, 628.
[32] Y. Yoshino, A. Iwabuchi, K. Noto, N. Sakai, M. Murakami, *Phys. C* **2001**, *357–360*, 796–798.